Bio-Design and Manufacturing (2024) 7:687–700
https://doi.org/10.1007/s42242-024-00306-1

RESEARCH ARTICLE

Microfluidic thermotaxic selection of highly motile sperm and in vitro fertilization

Sihan Chen[1] · Jiemin Chen[2] · Zihan Qin[3] · Jibo Wang[1] · Yuwen Wang[1] · Rong Liu[2] · Wen Zhao[1] · Ming Zhang[3] · Yuanzhen Zhang[3] · Mengcheng Luo[2,4] · Pu Chen[1,4]

Received: 2 January 2024 / Accepted: 18 June 2024 / Published online: 20 July 2024

Abstract

The selection of the most motile and functionally competent sperm is an essential basis for in vitro fertilization (IVF) and normal embryonic development. Widely adopted clinical approaches for sperm sample processing intensely rely on centrifugation and wash steps that may induce mechanical damage and oxidative stress to sperm. Although a few microfluidic sperm sorting devices may avoid these adverse effects by exploiting intrinsic guidance mechanisms of sperm swimming, none of these approaches have been fully validated by clinical-grade assessment criteria. In this study, a microfluidic sperm sorting device that enables the selection of highly motile and functional sperm via their intrinsic thermotaxis is presented. Bioinspired by the temperature microenvironment in the fallopian tube during natural sperm selection, a microfluidic device with controllable temperature gradients along the sperm separation channel was designed and fabricated. This study investigated the optimal temperature conditions for human sperm selection and fully characterized thermotaxis-selected sperm with 45 human sperm samples. Results indicated that a temperature range of 35–36.5 °C along the separation channel significantly improves human sperm motility rate ((85.25±6.28)% vs. (60.72±1.37)%; P=0.0484), increases normal sperm morphology rate ((16.42±1.43)% vs. (12.55±0.88)%; P<0.0001), and reduces DNA fragmentation ((7.44±0.79)% vs. (10.36±0.72)%; P=0.0485) compared to the nonthermotaxis group. Sperm thermotaxis is species-specific, and selected mouse sperm displayed the highest motility in response to a temperature range of 36–37.5 °C along the separation channel. Furthermore, IVF experiments indicated that the selected sperm permitted an increased fertilization rate and improved embryonic development from zygote to blastocyst. This microfluidic thermotaxic selection approach will be translated into clinical practice to improve the IVF success rate for patients with oligozoospermia and asthenozoospermia.

✉ Yuanzhen Zhang
zhangyuanzhen@whu.edu.cn

✉ Mengcheng Luo
luomengcheng@whu.edu.cn

✉ Pu Chen
puchen@whu.edu.cn

[1] Tissue Engineering and Organ Manufacturing (TEOM) Lab, Department of Biomedical Engineering, TaiKang Medical School (School of Basic Medical Sciences), Wuhan University, Wuhan 430071, China

[2] Hubei Provincial Key Laboratory of Developmentally Originated Disease, TaiKang Medical School (School of Basic Medical Sciences), Wuhan University, Wuhan 430071, China

[3] Reproductive Medicine Center, Zhongnan Hospital of Wuhan University, Wuhan 430071, China

[4] TaiKang Center for Life and Medical Sciences, Wuhan University, Wuhan 430071, China

Graphic abstract

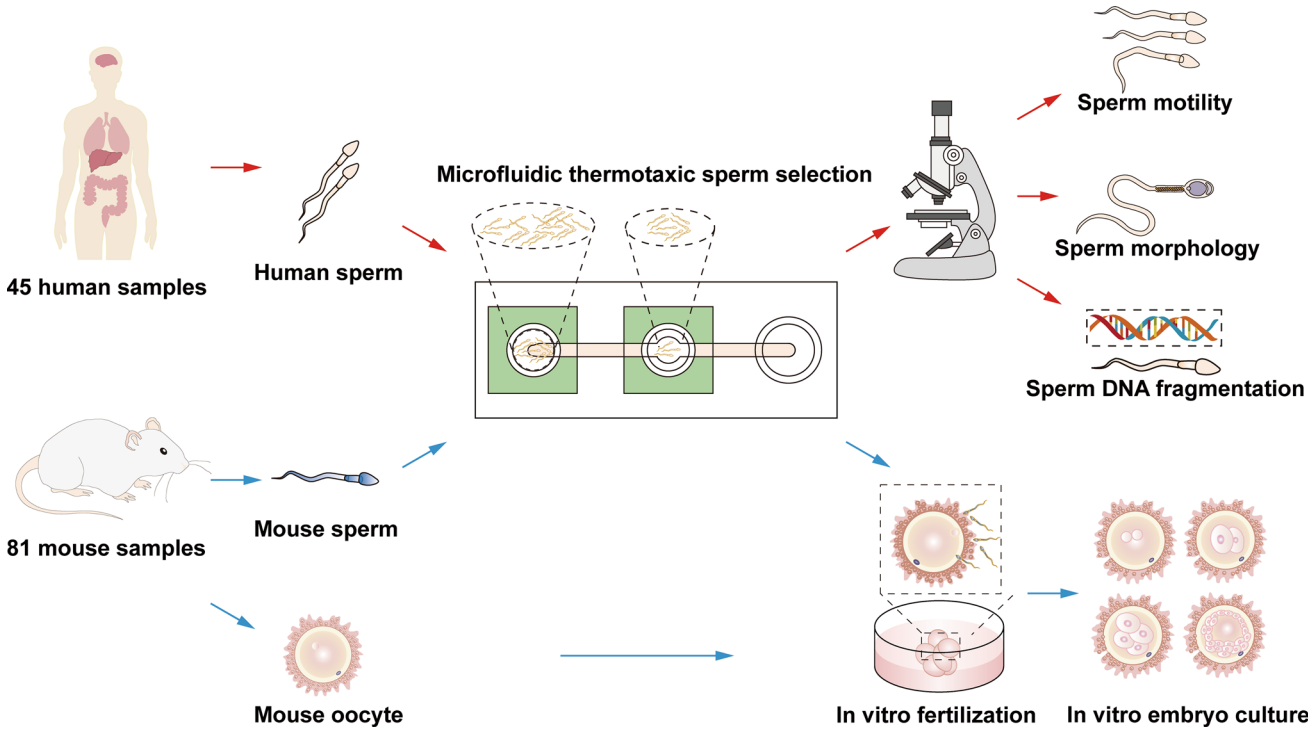

Keywords Microfluidic device · Thermotaxis · Sperm sorting · Assisted reproductive technology · In vitro fertilization

Introduction

Since the pioneering success of the first in vitro fertilization (IVF) procedure in 1978, IVF has emerged as the gold standard for assisted reproductive technology (ART), resulting in more than eight million IVF-conceived babies worldwide [1, 2]. Despite remarkable advancements in IVF techniques in the past four decades, the success rate of IVF procedures remains unsatisfactory. The rates of normal embryo development in vitro, embryo implantation, and pregnancy are between 30% and 50%, leading to a live birth rate of about 30% to 35% per fresh nondonor IVF cycle for women <35 years old [3]. Several major factors contribute to the failure of IVF, including embryo quality, egg and sperm quality, and uterine environment. Poor sperm quality is one of the major factors contributing to the failure of IVF, as sperm quality significantly impacts fertilization, embryo development, and subsequent embryo implantation [4, 5]. Widely adopted clinical standards for sperm selection in IVF employ methods such as sperm swim-up, density gradient, and simple washing. However, all these methods involve centrifugation as an essential step to separate motile sperm from debris or less motile sperm [6–9]. Although IVF procedures have made a compromise between separation efficiency and sperm quality by optimizing the centrifugation duration and acceleration, these procedures still could not select the most motile sperm or completely avoid potential mechanical and biochemical damage to sperm.

To address the above limitations, various passive sperm sorting approaches have been developed without centrifugation or wash steps. These approaches usually utilize the precise control of microfluidic flow, surface properties, microscale geometrical features, and microenvironmental gradients to isolate motile and morphologically normal sperm from semen samples [10–13]. Some of these approaches employ intrinsic mechanisms of sperm swimming and enrich motile sperm based on chemotaxis, rheotaxis, and thermotaxis [14–18]. Thermotaxis-based sperm sorting mimics the thermal microenvironment along the fallopian tube during natural sperm selection and isolates motile sperm from less motile or immotile sperm based on their responsiveness to temperature gradients. Compared to chemotaxis- or rheotaxis-based sperm selection methods, thermotaxis-based sperm selection methods do not require the addition of any chemoattractant or the precise control of microfluidic flow [19]. Thus, thermotaxic selection avoids potential biochemical damage to sperm and does not require professional skill or equipment for precise microfluidic

control. A few studies of thermotaxic selection of motile sperm have been reported using microfluidic devices. Li et al. reported a microfluidic device with a predesigned temperature gradient perpendicular to the microchannel to enrich motile human sperm [20]. They identified a mean percentage of thermoresponsive sperm of 11% when the temperature was 35 to 36.3 °C along the microchannel. Ko et al. demonstrated a microfluidic device to enrich motile mouse sperm based on thermotaxis [21]. Using integrated indium tin oxide (ITO) microheaters, a temperature gradient of 0.154 °C/mm was established along the microchannel. The optimal sperm enrichment was achieved under various inlet–outlet temperature ranges (35–37, 36–38, and 37–39 °C). However, few of these devices were fully validated with sufficient clinical samples and clinical-grade sperm assessment criteria. None of these studies have evaluated the selected sperm using IVF and embryo development assays. Thus, the clinical potential of thermotaxis-based microfluidic sperm sorting devices remains elusive.

In this study, a microfluidic device equipped with temperature control for the thermotaxic selection of motile sperm was developed (Fig. 1a). The optimal temperature ranges for selecting motile and functionally competent sperm were investigated using 45 human sperm samples. Sperm motility was evaluated by clinical-grade sperm motility criteria, including motility rate (M_R), curvilinear velocity (V_{CL}), straight-line velocity (V_{SL}), and average path velocity (V_{AP}), whereas sperm integrity was assessed using normal morphology rate (NMR) and DNA fragmentation index (DFI). The thermal gradient for enriching motile mouse sperm was investigated using 81 mouse samples. Sperm thermotaxis is species-specific. Finally, IVF was performed using enriched mouse sperm, and the fertilization, morula embryo formation, and blastocyst formation rates were evaluated. This study is a critical translational step to the clinical-grade application of thermotaxis-based microfluidic sperm selection for human IVF and ART.

Materials and methods

Device fabrication

The microfluidic device was constructed with two polyimide (PI) microheaters (Mingshenghua Technology Co., Ltd., China), three chambers, a polydimethylsiloxane (PDMS) layer, two ITO microheaters, and a glass slide (Fig. 1b). The device was fabricated using standard soft lithography. In brief, a 50-μm-thick layer of SU-8 photoresist (Microchem, Westborough, MA, USA) was coated and developed on a 4-inch silicon wafer, creating a channel template. The device was fabricated using PDMS (Sylgard 184; Dow Corning, USA) at a 10:1 volume ratio of base versus curing agent poured onto the silicon wafer, degassed, and cured at 80 °C for 2 h. After curing, the sample inlet chamber, collection chamber, and waste chamber were created using a punch (diameters of 2, 5, and 8 mm, respectively). The resulting channel was sealed on a glass slide using oxygen plasma and baked at 80 °C for 30 min before use.

Experimental setup

The experimental setup included a microfluidic chip, two switching power supplies (Mingwei, BS-10–5), two temperature sensors (Guankuan, WRNK-191), and two temperature controllers (Omron, E5CC-800). The switching power supply electrically drove the ITO microheaters. The temperature sensors monitored the temperature of ITO microheaters. The temperature controllers were used to tune the temperature of the sample inlet and collection chambers. Using these modules, a temperature feedback control system was built to sustain the temperature gradient along the sperm separation channel on the microfluidic chip (Fig. 1c).

Numerical simulation and experimental measurement of the temperature gradient

Numerical simulation of the temperature gradient along the sperm separation channel on a microfluidic chip was solved by a three-dimensional finite element model in COMSOL Multiphysics 6.0 (COMSOL, Inc., Burlington, MA, USA). The model was constructed by coupling multiple physics modules, including electric currents, heat transfer in solids, and joule heating. The physical properties of the chip materials for numerical calculation were obtained from the inbuilt material library of the software (Table 1). A stationary Joule heating simulation was conducted to visualize the temperature gradient (Fig. 2a). To replicate a physiological environment of the female reproductive tract, the effect of the input voltage value on the temperature gradient was numerically studied. Furthermore, an optotherm micro thermal imaging system (Hikmicro, H21pro) was employed to observe the temperature distribution on the separation channel (Fig. 2b).

Preparation of human and mouse sperm

A microfluidic sperm selection experiment was performed using deidentified discarded human semen samples from the Reproductive Medicine Center at the Zhongnan Hospital of Wuhan University, China. Forty-five human semen samples from healthy donors were used in this study. All sperm processing experiments were performed within 1 to 3 h after semen samples were collected from the clinical laboratory. Semen samples were incubated for 30 min at 37 °C to allow

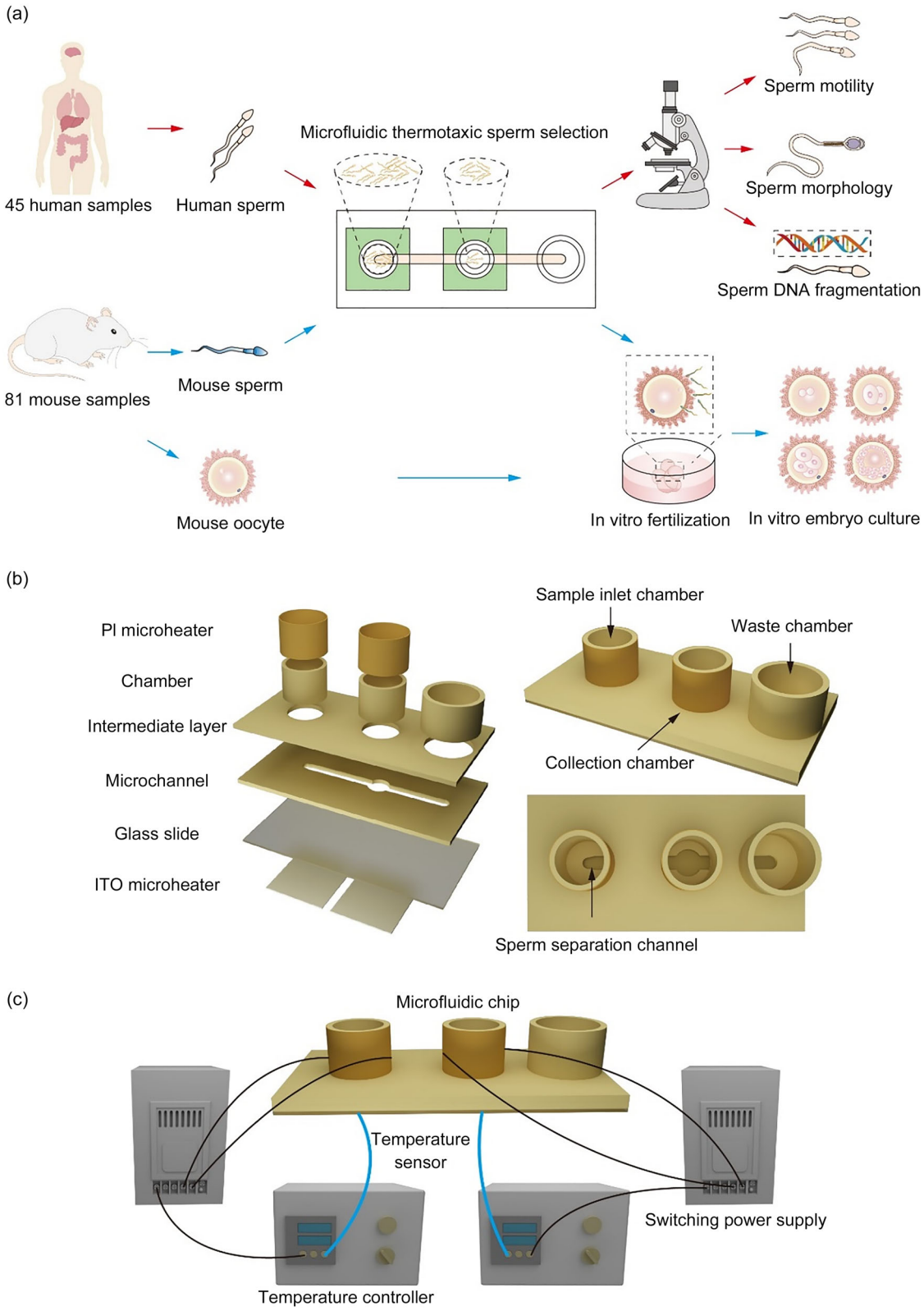

Fig. 1 Schematic view of a new microfluidic device for selecting highly motile sperm. **a** Schematic illustration of the experimental procedure. **b** Design of the microfluidic chip. **c** Experimental apparatus for the microfluidic device. PI: polyimide; ITO: indium tin oxide

Table 1 Parameters of the materials

Material	Density (kg/m^3)	Specific heat (J/(kg·K))	Thermal conductivity (W/(m·K))
ITO	7000	369.400	3.20
Glass wafer	2230	753.789	1.13
PDMS	970	1.460	0.15

ITO: indium tin oxide; PDMS: polydimethylsiloxane

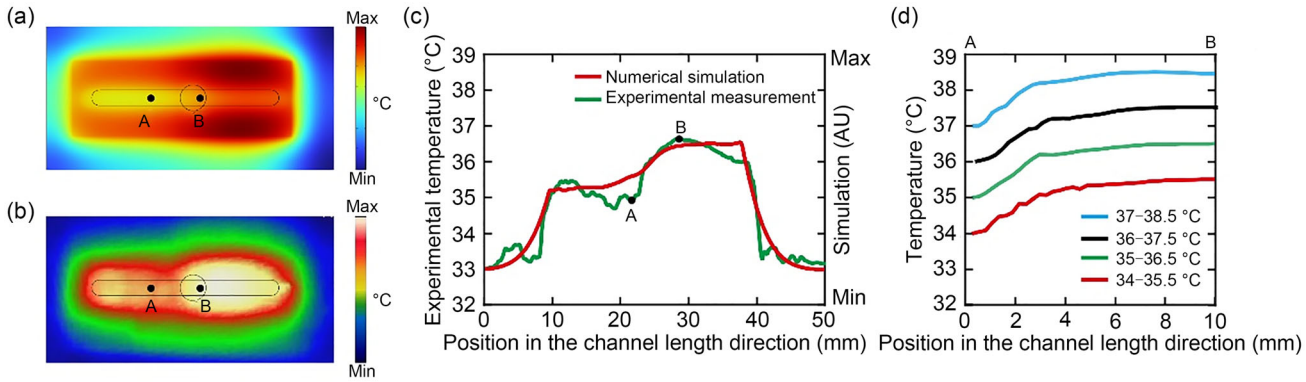

Fig. 2 Numerical simulation and experimental temperature distribution measurement on the microfluidic chip. **a** Numerical simulation of temperature distribution on the microfluidic chip. **b** IR thermography measurement of temperature distribution on the microfluidic chip. **c** Quantitative characterization of the temperature distribution along the sperm separation channel. **d** IR thermography measurement of the temperature distribution along the sperm separation channel under various temperature ranges (34–35.5, 35–36.5, 36–37.5, and 37–38.5 °C). IR: infrared

Table 2 Information on reagents

Reagent	Source	Identifier
HTF (human)	Vitrolife	G-IVF PLUS/60 mL-10136
Morphology staining kit	Anhui Anke Biotechnology	20,160,020
DFI staining kit	Anhui Anke Biotechnology	20,160,005
HTF (mouse)	Sigma	MR-070
Methylglyoxal	Sigma	M0205
PMSG	NSHF	11,008
HCG	NSHF	11,025
KSOM	Sigma	MR-10

HTF: human tubal fluid; DFI: DNA fragmentation index; PMSG: pregnant mare serum gonadotropin; HCG: human chorionic gonadotropin; KSOM: potassium simplex optimization medium; NSHF: Ningbo Second Hormone Factory

liquefaction. Sperm samples were added to the appropriate amount of human tubal fluid (HTF; Vitrolife, G-IVF PLUS/60 mL-10136) and incubated under an atmosphere of 5% CO_2 at 37 °C for 1 h to undergo capacitation (Table 2).

For mouse sperm sorting experiments, 3-month-old C57BL/6 male mice were euthanized by cervical dislocation, and mouse semen samples were collected from the caudal epididymis and suspended in HTF (Sigma, MR-070) supplemented with 500 μmol/L methylglyoxal (Sigma, M0205). Mouse sperm samples were incubated under an atmosphere of 5% CO_2 at 37 °C for 1 h to undergo capacitation. All efforts were made to minimize animal suffering and reduce the number of animals used in the experiments.

Mouse oocyte collection

Metaphase II oocytes were obtained from the fallopian tubes of 4- to 6-week-old female mice (C57BL/6) through superovulation after injection of 5 IU PMSG Ningbo Second Hormone Factory (NSHF) and an equivalent dose of HCG (NSHF) over 48 h. Fourteen hours after HCG administration, fallopian tubes were extracted from super ovulated female

mice and placed in an M2-containing Petri dish at room temperature. After a wash, fallopian tubes were transferred to a fresh M2 medium, and cumulus-oocyte complexes (COCs) were released from the ampulla using a 1 mL syringe needle. COCs were transferred into 0.1% hyaluronidase for digestion at 37 °C for 3 to 4 min. Eggs with digested and removed cumulus cells were swiftly picked up with an egg-picking needle. Normal (full and bright) metaphase II oocytes were selected and washed to eliminate residual cumulus cells and hyaluronidase with HTF medium three to four times.

In vitro fertilization

Fertilization drops were prepared with 5 mL HTF, covered with mineral oil, and preincubated overnight at 37 °C in a 5% CO_2 atmosphere. Groups of 10 to 15 metaphase II oocytes were placed in each drop. Subsequently, 5 μL fresh epididymal sperm was added to the fertilization drop to achieve a final concentration of 1×10^6 sperm/mL, and the drop was incubated for 6 h at 37 °C in a humidified atmosphere of 5% CO_2. Finally, oocytes were washed with KSOM (Sigma, MR-10).

In vitro embryo culture

The embryos were cultured to the desired stages (dividing egg, morula, and blastocyst stages) in groups of 10 to 15 embryos in 25 μL drops of KSOM, covered with mineral oil, and placed in an incubator at 37 °C in a humidified atmosphere of 5% CO_2.

Analysis of sperm motility

Microfluidic thermotaxic selection of sperm (thermotaxis group) was evaluated with two control groups. The nonsorting group included capacitated sperm without microfluidic sperm sorting, and the nonthermotaxis group included microfluidic selected capacitated sperm in the collection chamber by free swimming without thermotaxic guidance. Sperm motility was analyzed by the motility module in a clinical-grade multiparameter sperm quality analysis system (BEION, V4.20). The selected sperm in the collection chamber were transferred to a glass slide, and the sperm swimming pattern was recorded for quantitative analysis of four motility parameters, including M_R, V_{CL}, V_{SL}, and V_{AP}. M_R was defined as the percentage of motile sperm in the given sample. V_{CL} was defined as the average speed of a sperm along its actual curving path. V_{SL} was defined as the speed of a sperm moving along a straight path. V_{AP} was defined as the average speed of a sperm along its trajectory. Furthermore, the motile sperm are characterized by their ability to move actively. V_{CL}, V_{SL}, and V_{AP} were obtained by analyzing sperm trajectories in Video S1 (Supplementary Information).

Sperm morphology

The World Health Organization manual guidelines were strictly followed to examine sperm morphology. The sperm staining detection kit (Anhui Anke Biotechnology, 20,160,020) was used to stain all sperm components (acrosome, head, midpiece, and main piece of tail) differentially in different intensities of blue. The morphology of the stained sperm was quantitatively analyzed using the morphology module in the sperm quality analysis system (BEION, V4.20).

Assessment of sperm DNA fragmentation

The DFI of sperm was evaluated utilizing the sperm DNA fragment staining kit (Anhui Anke Biotechnology, 20,160,005) according to the manufacturer's instructions. Sperm with very small halos, without halos, and without halo degraded contained fragmented DNA. Sperm with medium to large halos contained intact DNA. The stained sperm were quantitatively analyzed using the DFI module in the sperm quality analysis system (BEION, V4.20). At least 100 sperm were assessed for each sample, with nine samples in each group.

Immunofluorescence staining

Mouse embryo samples were fixed overnight in 4% paraformaldehyde, followed by phosphate-buffered saline (PBS) washes. Blocking was performed using 5% goat serum. Permeabilization was performed using PBS containing 0.2% Triton X-100 for 30 min, followed by PBS washes. The embryos were incubated overnight with either anti-OCT4 (Abcam, 19,857) or anti-CDX2 (Abcam, 227,201) primary antibodies. After removing the primary antibodies, the samples underwent PBS washes. The embryos were incubated with secondary antibodies conjugated with Alexa Fluor 488 or 546 (red) at room temperature for 60 min, followed by PBS washes. Cell nuclei were stained with 4′,6-diamidino-2-phenylindole (1 mg/mL) for 5 min, followed by PBS washes. Finally, the embryos were mounted on glass slides using a mounting medium. The stained embryos were imaged under a fluorescence microscope (Leica, TCS SP8).

Statistical analysis

Data as the mean±standard error were quantified from at least three independent experiments. *P* values were determined using one-way analysis of variance or Student's *t*-test to verify statistically significant differences among groups. All collected data were graphed and analyzed using the statistical software GraphPad Prism 8.0.0 (GraphPad Software, San Diego, CA, USA).

Results

Characterization of the temperature gradient on a microfluidic chip

The temperature distribution along the sperm separation channel on the microfluidic chip was visualized through numerical simulation and infrared (IR) thermography measurement (Figs. 2a and 2b). When ITO microheaters were set to 35 °C in point A and 36.5 °C in point B, there was a sharp temperature gradient between these two areas. Furthermore, quantitative analysis of the temperature gradient along the channel indicated that the simulation results were consistent with the experimental results, and the temperature gradient was established with an average of 0.15 °C/mm (Fig. 2c) along the 10-mm long separation channel between the sample inlet chamber and the collection chamber. Temperature ranges (34–35.5, 35–36.5, 36–37.5, and 37–38.5 °C) along the separation channel were experimentally set up using the temperature feedback control system.

Thermotaxic response of human sperm under different temperature ranges

The thermotaxic response of human sperm in various temperature ranges along the separation channel (34–35.5, 35–36.5, 36–37.5, and 37–38.5 °C) was investigated. All these conditions in the thermotaxis group demonstrated a significantly higher level (P<0.0001) of sperm motility than the nonsorting group in all four clinical-grade motility criteria, including M_R, V_{CL}, V_{SL}, and V_{AP} (Fig. 3). Sperm motility from 35 to 36.5 °C displayed the highest increase over the nonsorting group, with mean M_R (164%), V_{CL} (97%), V_{SL} (125%), and V_{AP} (99%) among these temperature ranges. Sperm selected by this temperature range demonstrated significantly higher motility than those sperm at other temperature ranges (34–35.5, 36–37.5, and 37–38.5 °C) in nearly all four clinical-grade motility criteria.

Evaluation of thermotaxis-selected human sperm

Comparative analysis was performed on thermotaxis-selected sperm from 35 to 36.5 °C in the nonthermotaxis and nonsorting groups in terms of motility, morphology, and DNA integrity (Fig. 4a). The concentration of thermotaxis-selected sperm in the collection chamber was $(3.46\pm0.30)\times10^6$ sperm/mL in the experiments, whereas the initial concentration of motile sperm in the inlet chamber was $(49.19\pm1.72)\times10^6$ sperm/mL. Thus, a 7.03% fold enrichment of motile sperm was obtained via microfluidic thermotaxis-based selection. The average M_R of sperm in the thermotaxis group was (85.25±6.28)%, which was much higher than those in the nonthermotaxis and nonsorting groups (Fig. 4b). Furthermore, sperm in the thermotaxis group showed higher V_{CL}, V_{SL}, and V_{AP} than those in the nonsorting and nonthermotaxis groups.

Morphological analysis was performed on thermotaxis-selected sperm, and their DNA integrity was further examined. Thermotaxis-selected sperm demonstrated an NMR of (16.42±1.43)%, which was significantly higher than those in the nonthermotaxis (12.55±0.88)% and nonsorting (5.10±0.60)% groups (Fig. 4c). Thermotaxis-selected sperm displayed significantly lower DFI (7.44±0.79)% than those in nonthermotaxis (10.36±0.72)% and nonsorting (15.10±0.98)% groups (Fig. 4d). These results indicated that microfluidic thermotaxic selection significantly improves sperm quality in terms of motility, morphology, and DNA integrity.

Thermotaxic response of mouse sperm under different temperature ranges

The thermotaxic response of mouse sperm was investigated in various temperature ranges (34–35.5, 35–36.5, 36–37.5, and 37–38.5 °C) along the separation channel. All thermotaxis groups displayed a significantly higher level (P<0.0001) of sperm motility than the nonsorting group in terms of M_R, V_{CL}, V_{SL}, and V_{AP} (Fig. 5). Thermotaxic selection from 36 to 37.5 °C displayed the highest increase over the nonsorting group in terms of mean M_R (119%), V_{CL} (84%), V_{SL} (120%), and V_{AP} (112%). Sperm selected under this temperature range also demonstrated significantly higher motility than those under the other temperature ranges. The concentration of thermotaxis-selected sperm in the collection chamber was $(4.42\pm0.15)\times10^6$ sperm/mL in the experiments, whereas the initial concentration of motile sperm in the inlet chamber was $(41.89\pm1.68)\times10^6$ sperm/mL. Thus, there was a 10.55% fold enrichment of motile sperm via the microfluidic thermotaxic selection. This optimal temperature range is species-specific for mouse sperm thermotaxis, as the optimal temperature range for human sperm thermotaxis is 35 to 36.5 °C.

IVF using thermotaxis-selected sperm

The functionality of thermotaxis-selected mouse sperm was investigated using a standard mouse IVF procedure (n=3). Bright-field imaging analysis indicated that thermotaxis-selected and nonsorting sperm enable a normal early-stage embryonic development from fertilization to blastocyst production (Fig. 6a). The thermotaxis group displayed an increase in mean rates of egg division (33%), morula formation (24%), and blastocyst production (19%) over the nonsorting group (Fig. 6b). There were no statistically significant differences in fertilization, morula, and blastocyst

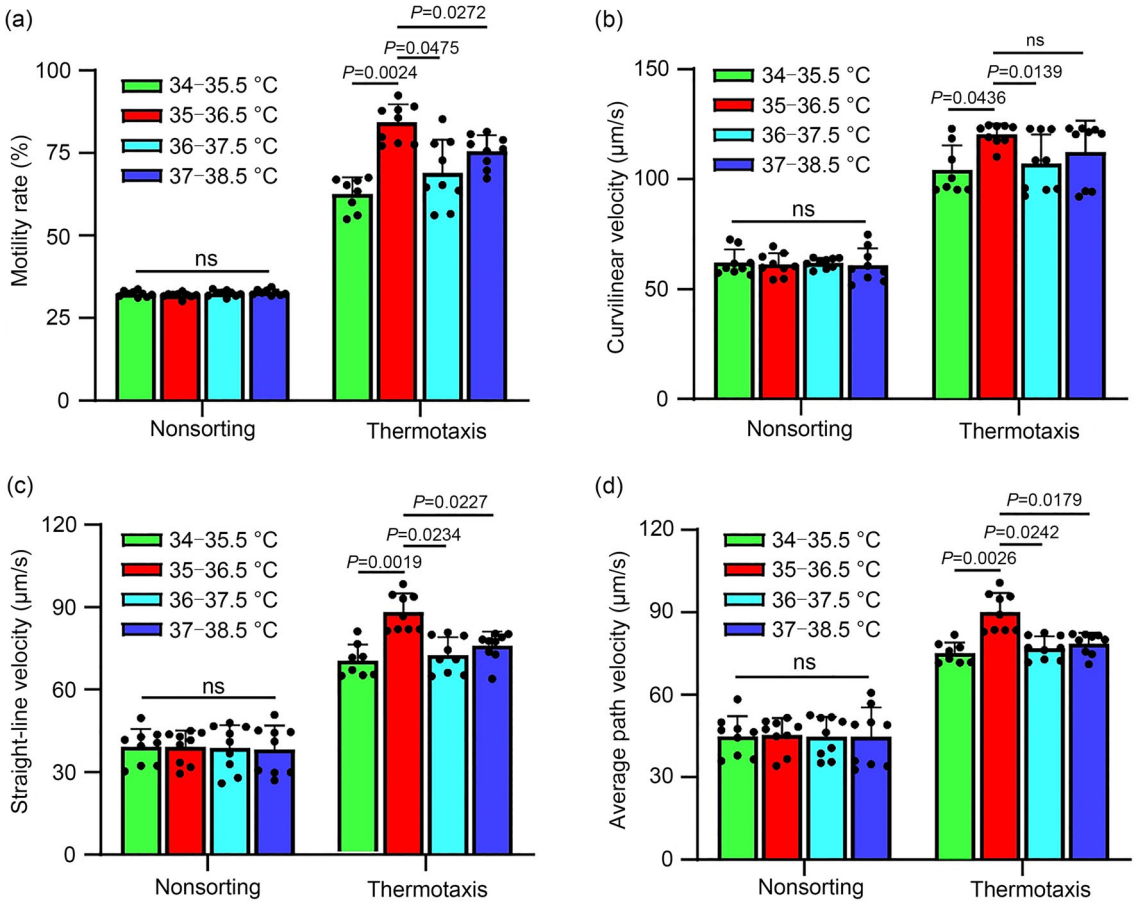

Fig. 3 Human sperm motility under various temperature ranges. Human sperm motility was examined on the thermotaxis and nonsorting groups under various temperature ranges (34–35.5, 35–36.5, 36–37.5, and 37–38.5 °C). **a** Motility rate. **b** Curvilinear velocity. **c** Straight-line velocity. **d** Average path velocity. Data are expressed as mean±standard error (n=3). ns: non-statistical significance

rates between the two groups. This lack of significance can be attributed to the utilization of sperm from normal mice for selection purposes. Sperm M_R of the wild-type mice utilized in this study exceeded 40%, which was sufficient for IVF of mouse eggs. Furthermore, blastocysts derived from the thermotaxis group were characterized. Immunofluorescence staining indicated Oct4 (a pluripotent stem cell marker) and Cdx2 (a marker for trophectoderm) expression in blastocysts, suggesting the potential to differentiate into three germ layers and trophectoderm after embryo implantation (Fig. 6c).

Discussion

Male infertility is responsible for about 40% to 50% of all human infertility cases and affects approximately 10% of men worldwide [22]. One of the primary causes of male infertility is abnormal sperm production or function. Low sperm count, known as oligospermia, can reduce the chances of successful fertilization. Poor sperm motility (asthenospermia) or abnormal sperm shape and structure (teratospermia) can impede sperm from reaching and penetrating the egg. In the past decades, ART (such as IVF and intracytoplasmic sperm injection) and sperm retrieval procedures (such as testicular sperm extraction (TESE) or microdissection TESE) have addressed certain male infertility issues [23–26]. IVF techniques, mainly including sperm swim-up, density gradient, and simple washing, are clinical standards for selecting viable and motile sperm and are widely adopted in reproductive medicine centers. These techniques employ active operations such as centrifugation and washing to handle semen. Despite the advantages of accessibility, ease of operation, and cost-effectiveness, these techniques suffer from some drawbacks, including limited motile sperm selection, mechanical damage, and oxidative stress to DNA integrity, which are partially responsible for the failure of IVF and abnormal embryogenesis. Thermotaxis-based sperm sorting mimics the thermal microenvironment along the fallopian tube during natural sperm selection and isolates motile sperm

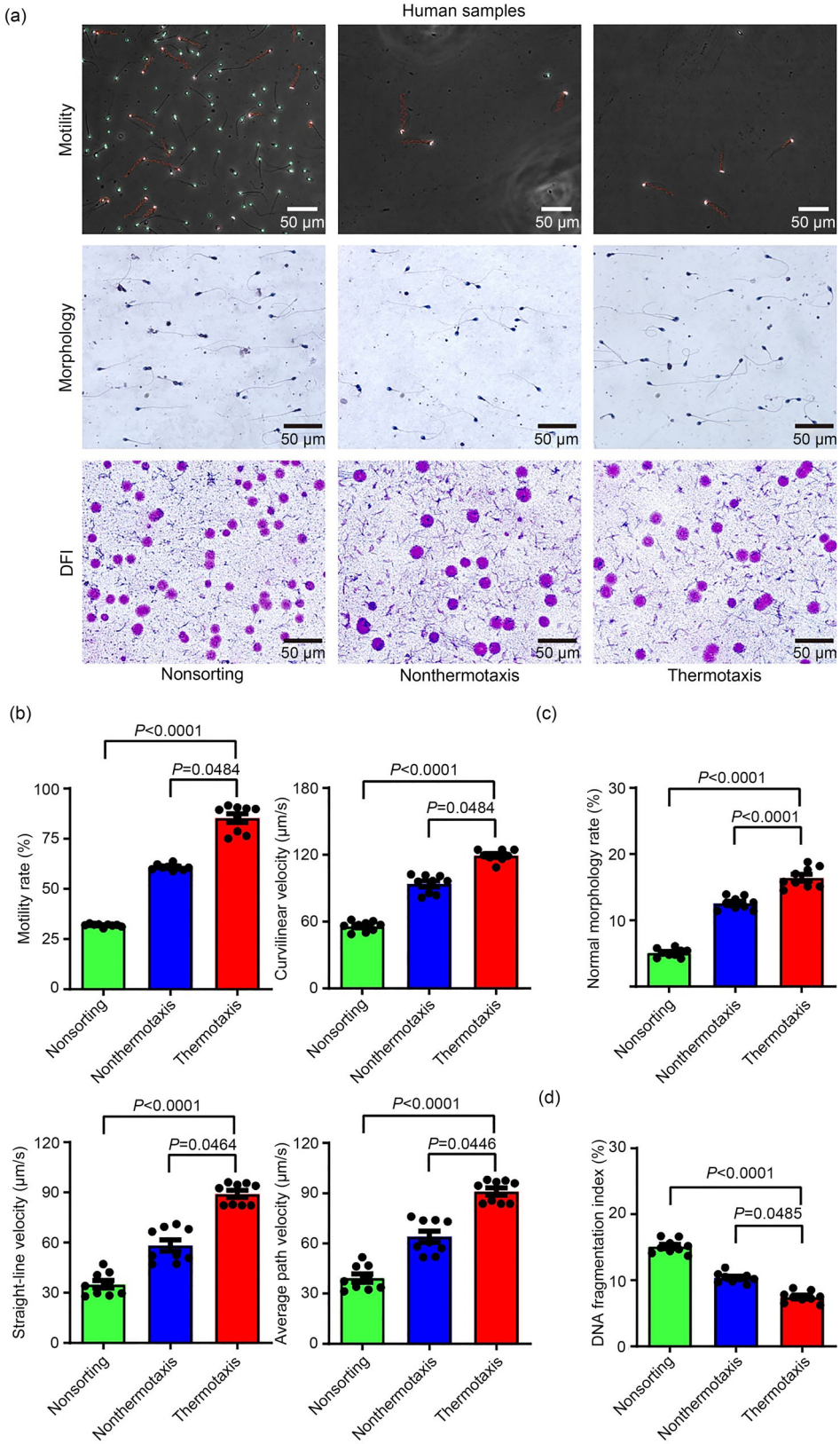

Fig. 4 Comparison of thermotaxis-selected human sperm with sperm in the nonthermotaxis and nonsorting groups. **a** Representative images of sperm movement trajectories, sperm morphology, and DNA fragmentation assay (DFI). **b** Sperm motility analysis of motility rate, curvilinear velocity, straight-line velocity, and average path velocity. **c** Sperm morphology analysis. **d** DNA fragmentation analysis of sperm cells. Data are expressed as mean±standard error (n=3)

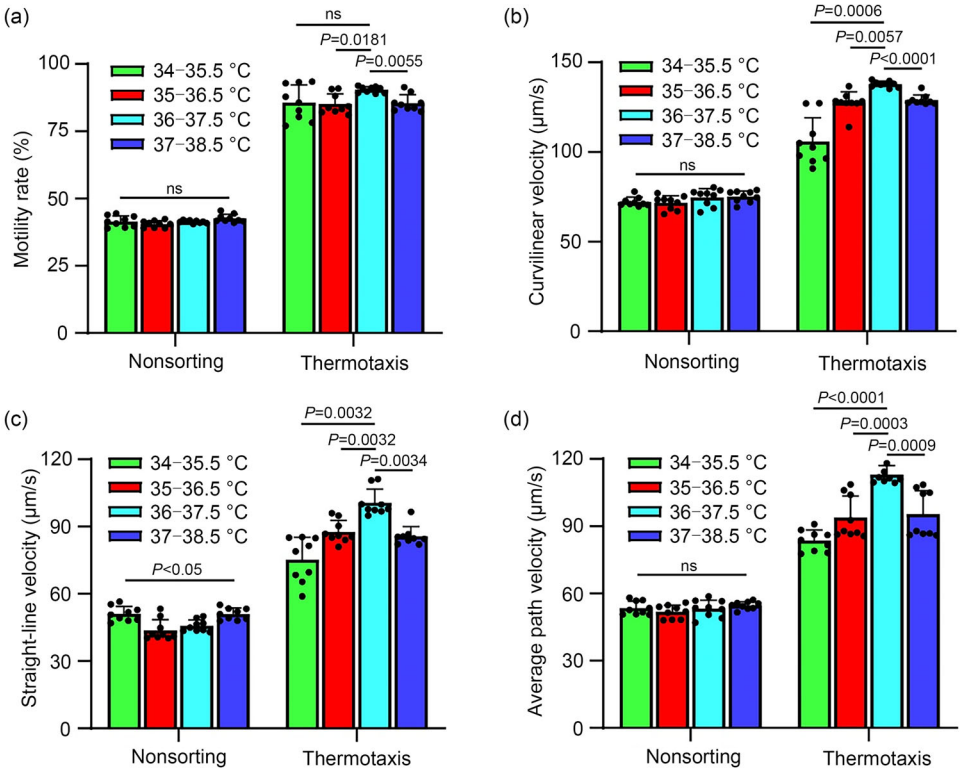

Fig. 5 Mouse sperm motility under various temperature ranges. Mouse sperm motility was examined on the thermotaxis and nonsorting groups under various temperature ranges (34–35.5, 35–36.5, 36–37.5, and 37–38.5 °C). **a** Motility rate. **b** Curvilinear velocity. **c** Straight-line velocity. **d** Average path velocity. Data are expressed as mean±standard error (n=3)

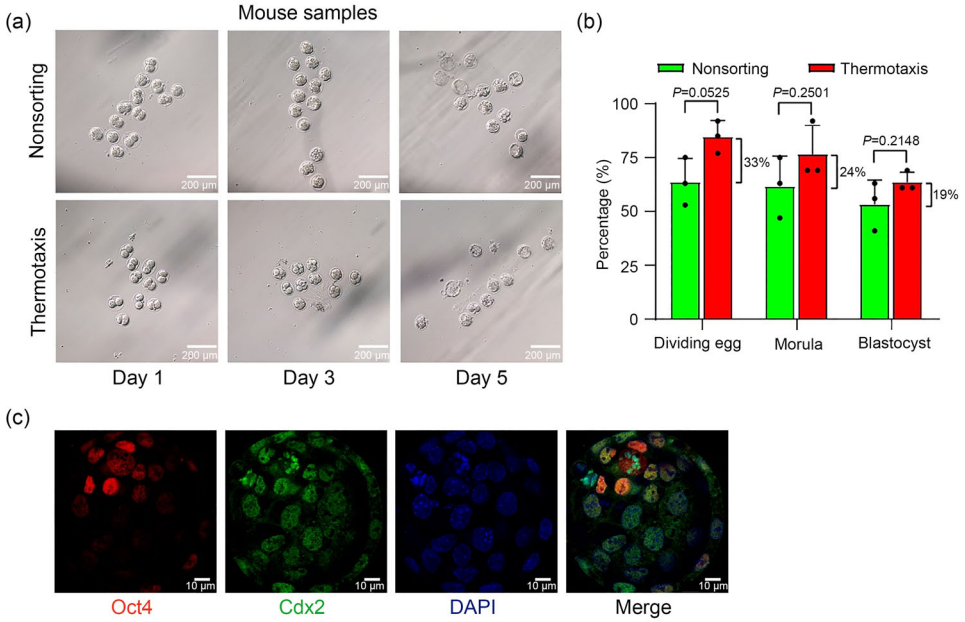

Fig. 6 Characterization of thermotaxis-selected mouse sperm for IVF. **a** Representative images of embryos on Days 1, 3, and 5 after fertilization were examined by optical microscopy. **b** Successful rate of early-stage embryonic development from fertilization to blastocyst stages. **c** Representative immunofluorescence staining images of the embryo on Day 7 after fertilization. Data are expressed as mean±standard error (n=3). IVF: in vitro fertilization; DAPI: 4',6-diamidino-2-phenylindole

from less motile or immotile sperm based on their responsiveness to the temperature gradient. This selection method via thermotaxis bypasses potential biochemical damage to sperm, offering a gentler alternative for sperm sorting.

In natural sperm selection and fertilization, motile sperm cells display intrinsic capacity to navigate their directions and swim along the female genital tract toward the egg [27]. Some key mechanisms of natural sperm navigation have been elucidated in the past decades, including chemotaxis, rheotaxis, and thermotaxis [28–32]. Thermotaxis may influence sperm movement within the female reproductive tract, particularly in the vicinity of the oviducts. Human and mouse sperm may have evolved distinct thermotaxic responses to the temperature gradient due to differences in

their reproductive physiology and environmental conditions. Sperm sensitivity to temperature changes varies depending on the species' natural habitats and reproductive strategies. The expression levels and types of thermosensitive proteins in sperm vary between species. These proteins play crucial roles in detecting temperature changes and initiating cellular responses. Differences in the expression or functionality of thermosensitive proteins may contribute to variations in thermotaxic responses between human and mouse sperm. Sperm exhibit thermotaxic responses and move toward warmer reproductive tract regions, such as the fallopian tubes, where fertilization usually occurs [33]. Bahat et al. discovered that human sperm could respond to a temperature gradient by thermotaxis [34]. Furthermore, Boryshpolets et al. identified that sperm direct their swimming in the direction of the thermal gradient by modulating the frequency of turns and speed [35]. Bahat, Eisenbach, and Giojalas suggested that sperm thermotaxis relied on inositol 1,4,5-triphate receptor (IP3R) Ca^{2+} channels located in internal Ca^{2+} stores [36, 37]. The thermotaxic responses of sperm are mediated by phospholipase C and request intracellular rather than extracellular Ca^{2+} concentration. The mechanism of thermotaxis is independent of chemotaxis receptors, indicating the potential of simultaneously exploring thermotaxis and chemotaxis in sperm selection. Two proteins, G protein-coupled receptors and ion channels, are involved in sensory transduction in eukaryotes [38, 39]. Opsins and thermosensitive transient receptor potential (thermoTRP) channels are currently under investigation as potential sensors for thermotaxis. ThermoTRP channels, a subgroup of the TRP superfamily, are highly sensitive to temperature changes and help regulate body temperature [40, 41] and include TRPV1–4, TRPM8, TRPA1, and others. Opsins, traditionally associated with light detection in tissues like the eyes and skin, have been detected in other organs and may have light-independent effects. In sperm, thermoTRP channels such as TRPV1, TRPV4, and TRPM8 are candidates for temperature sensors [42]. Opsins, including rhodopsin and melanopsin, have also been identified in sperm and may play a role in thermotaxis. These proteins initiate signaling cascades similar to those in visual cells, enabling sperm to sense temperature variations [43, 44].

Inspired by sperm intrinsic thermotaxis, a thermotaxis-based microfluidic device for motile sperm selection and IVF was designed and fabricated. A temperature control system with a feedback loop was constructed to precisely create and sustain a temperature gradient along the sperm separation channel. The system contained an ITO glass heater at the substrate [45], two flexible PI microheaters tightly surrounding the sample inlet and collection chambers, and temperature sensors at the bottom of these two chambers. Previous studies reported thermotaxis-based microfluidic devices for sperm selection, and these devices usually create thermal gradients solely using integrated ITO heaters or resistive heaters on an aluminum alloy tank for heat dissipation. Compared to these devices, our device enables a robust thermal gradient and a clear substrate for in situ sperm observation.

Previous studies revealed a temperature difference of 1 to 2 °C between the sperm storage site and the fertilization site, and the temperature difference is ovulation-dependent [46, 47]. Human sperm can respond to temperature gradients as low as 0.014 °C/mm over a broad temperature range (29–41 °C). In this study, a fixed temperature difference of 1.5 °C was predefined from the inlet chamber to the collection chamber, and sperm motility was investigated under various temperature ranges. An optimal temperature range of 35 to 36.5 °C was identified along the sperm separation channel with a thermal gradient of 0.15 °C/mm for microfluidic thermotaxic selection of highly motile sperm. Our device was fully validated with 45 human semen samples from patients with normal sperm motility. Microfluidic thermotaxic selection significantly improved sperm motile parameters compared to the free swimming group (nonthermotaxis) in terms of M_R ((85.25±6.28)% vs. (60.72±1.37)%; P=0.0484), V_{CL} ((119.33±4.82) vs. (93.79±7.64) μm/s; P=0.0484), V_{SL} ((89.10±6.11) vs. (58.28±9.60) μm/s; P=0.0464), and V_{AP} ((91.07±6.21) vs. (64.03±9.49) μm/s; P=0.0446). Microfluidic thermotaxic selection ensures a higher NMR ((16.42±1.43)% vs. (12.55±0.88)%; P<0.0001) and a lower DFI ((7.44±0.79)% vs. (10.36±0.72)%; P=0.0485) than the nonthermotaxis and nonsorting groups. Li et al. [20] and Ko et al. [21] separately demonstrated a microfluidic device design for the thermotaxic selection of human sperm. However, these devices have not been assessed for sperm motile parameters, sperm morphology, and DNA integrity. Thus, our microfluidic device cannot be quantitatively compared to these reported devices in terms of the performance of human motile sperm selection. Yan et al. reported a microfluidic device with combined thermotaxis and chemotaxis for sperm selection [48]. Compared to their device, our device offers a comparable enriched sperm number (8000 vs. 10000) with similar sperm motility (V_{CL} 125 vs. 120 μm/s and V_{SL} 80 vs. 100 μm/s) in an affordable sorting time (20 vs. 15 min). Our microfluidic device showed similar performance in enriched sperm number and motility compared to previously reported devices. However, our current design has limitations, mainly relying on thermotaxis for sperm selection. Integrating chemotaxis into the same microfluidic chip could more accurately replicate the sperm sorting process in the reproductive tract in vivo, potentially enhancing sperm sorting efficiency.

Sperm thermotaxis is species-specific, and the optimal mouse sperm motility is achieved from 36 to 37.5 °C, distinct from the optimal temperature range (35–36.5 °C) for human sperm selection. Furthermore, the functionality of selected mouse sperm was evaluated for fertilization and embryonic

development. Results indicated that the thermotaxis-selected sperm enables a higher rate of egg division. Thermotaxis-selected sperm demonstrated higher mean morula and blastocyst formation rates in embryogenesis than nonsorting sperm. Immunostaining confirmed spatially differentiated Oct4 and Cdx2 expression in blastocysts. Oct4 indicates pluripotency for generating three germ layers, and Cdx2 is the core transcription factor responsible for trophectoderm development. This staining suggested the potential of normal embryogenesis after blastocyst implantation. These IVF validations have never been reported in previous thermotaxis- or chemotaxis-based microfluidic devices.

Conclusions

In this study, a biomimetic microfluidic device was developed to isolate highly motile sperm based on thermotaxic guidance. The device contains a temperature control system with a feedback loop to precisely create and sustain a robust temperature gradient for the thermotaxic selection of sperm. The device is fully characterized with clinical human semen samples and criteria. Thermotaxis-sorted sperm exhibited enhanced motility and reduced DFI compared to the non-thermotaxis group, and mouse sperm IVF assays further implied the potential of this device to increase the success rate in human IVF. Overall, this study will supplement as an essential step to translate thermotaxis-based microfluidic sperm sorting devices into clinical-grade applications and improve IVF success rate for patients with oligozoospermia and asthenozoospermia.

Supplementary Information The online version contains supplementary material available at https://doi.org/10.1007/s42242-024-00306-1.

Acknowledgements This work was supported by the Key Research and Development Project of Hubei Province, China (No. 2021BCA111). The authors would like to thank Yumin Cao and Wenhao Xu from Zhongnan Hospital of Wuhan University for their assistance in the experimental operation.

Author contributions Conceptualization was contributed by PC, YZZ, and MCL. Data curation was contributed by SHC, JMC, ZHQ, and PC. Formal analysis was contributed by ZHQ and SHC. Funding acquisition was contributed by PC, YZZ, and MCL. Investigation was contributed by SHC, JMC, and ZHQ. Methodology was contributed by SHC. Project administration was contributed by PC, YZZ, and MCL. Resources were contributed by PC, YZZ, MCL, and MZ. Software was contributed by SHC and JBW. Supervision was contributed by PC, YZZ, and MCL. Validation was contributed by SHC, JMC, ZHQ, WZ, JBW, and PC. Visualization was contributed by SHC, YWW, and JBW. Writing—original draft was contributed by SHC and PC. Writing—review and editing was contributed by PC, WZ, and RL.

Data availability All data needed to evaluate the conclusions are present in the paper and the supplementary materials. Additional data related to this paper may be requested from the authors.

Declarations

Conflict of interest The authors declare that they have no conflict of interest.

Ethical approval An exempt human subject protocol (ID: 2022013K) was approved by the Medical Ethics Committee at the Zhongnan Hospital of Wuhan University, and informed consent was obtained from all donors. Experimental procedures involving animals were conducted in accordance with ethical standards and approved by the Center for Animal Experiments at Wuhan University. The Animal Using Protocol Number for this study is [WP20230510].

References

1. Zubizarreta ME, Xiao S (2020) Bioengineering models of female reproduction. Bio-Des Manuf 3(3):237–251. https://doi.org/10.1007/s42242-020-00082-8
2. Yu SX, Wu Y, Luo H et al (2023) Escaping behavior of sperms on the biomimetic oviductal surface. Anal Chem 95(4):2366–2374. https://doi.org/10.1021/acs.analchem.2c04338
3. Baldini D, Ferri D, Baldini GM et al (2021) Sperm selection for ICSI: do we have a winner? Cells 10(12):3566. https://doi.org/10.3390/cells10123566
4. Giojalas LC, Guidobaldi HA (2020) Getting to and away from the egg, an interplay between several sperm transport mechanisms and a complex oviduct physiology. Mol Cell Endocrinol 518:110954. https://doi.org/10.1016/j.mce.2020.110954
5. Suarez SS (2016) Mammalian sperm interactions with the female reproductive tract. Cell Tissue Res 363(1):185–194. https://doi.org/10.1007/s00441-015-2244-2
6. Nikshad A, Aghlmandi A, Safaralizadeh R et al (2021) Advances of microfluidic technology in reproductive biology. Life Sci 265:118767. https://doi.org/10.1016/j.lfs.2020.118767
7. Dadkhah E, Hajari MA, Abdorahimzadeh S et al (2023) Development of a novel cervix-inspired tortuous microfluidic system for efficient, high-quality sperm selection. Lab Chip 23(13):3080–3091. https://doi.org/10.1039/d3lc00037k
8. Anbari F, Khalili MA, Sultan Ahamed AM et al (2021) Microfluidic sperm selection yields higher sperm quality compared to conventional method in ICSI program: a pilot study. Syst Biol Reprod Med 67(2):137–143. https://doi.org/10.1080/19396368.2020.1837994
9. Nosrati R, Graham PJ, Zhang B et al (2017) Microfluidics for sperm analysis and selection. Nat Rev Urol 14(12):707–730. https://doi.org/10.1038/nrurol.2017.175
10. Hsu CT, Lee CI, Lin FS et al (2023) Live motile sperm sorting device for enhanced sperm-fertilization competency: comparative analysis with density-gradient centrifugation and microfluidic sperm sorting. J Assist Reprod Genet 40(8):1855–1864. https://doi.org/10.1007/s10815-023-02838-4
11. Mirsanei JS, Sheibak N, Zandieh Z et al (2022) Microfluidic chips as a method for sperm selection improve fertilization rate in couples with fertilization failure. Arch Gynecol Obstet 306(3):901–910. https://doi.org/10.1007/s00404-022-06618-w
12. Doostabadi MR, Mangoli E, Marvast LD et al (2022) Microfluidic devices employing chemo- and thermotaxis for sperm selection can improve sperm parameters and function in patients with high DNA fragmentation. Andrologia 54(11):e14623. https://doi.org/10.1111/and.14623
13. Štiavnická M, Abril-Parreño L, Nevoral J et al (2017) Non-invasive approaches to epigenetic-based sperm selection. Med Sci Monit 23:4677–4683. https://doi.org/10.12659/msm.904098

14. Ruiz-Díaz S, Mazzarella R, Navarrete-López P et al (2023) Bull spermatozoa selected by thermotaxis exhibit high DNA integrity, specific head morphometry, and improve ICSI outcome. J Anim Sci Biotechnol 14(1):11. https://doi.org/10.1186/s40104-022-00810-3
15. Berendsen JTW, Kruit SA, Atak N et al (2020) Flow-free microfluidic device for quantifying chemotaxis in spermatozoa. Anal Chem 92(4):3302–3306. https://doi.org/10.1021/acs.analchem.9b05183
16. Ma R, Xie L, Han C et al (2011) In vitro fertilization on a single-oocyte positioning system integrated with motile sperm selection and early embryo development. Anal Chem 83(8):2964–2970. https://doi.org/10.1021/ac103063g
17. Cho BS, Schuster TG, Zhu X et al (2003) Passively driven integrated microfluidic system for separation of motile sperm. Anal Chem 75(7):1671–1675. https://doi.org/10.1021/ac020579e
18. Olatunji O, More A (2022) A review of the impact of microfluidics technology on sperm selection technique. Cureus 14(7):e27369. https://doi.org/10.7759/cureus.27369
19. Pérez-Cerezales S, Laguna-Barraza R, Castro AC et al (2018) Sperm selection by thermotaxis improves ICSI outcome in mice. Sci Rep 8(1):2902. https://doi.org/10.1038/s41598-018-21335-8
20. Li Z, Liu W, Qiu T et al (2014) The construction of an interfacial valve-based microfluidic chip for thermotaxis evaluation of human sperm. Biomicrofluidics 8(2):024102. https://doi.org/10.1063/1.4866851
21. Ko YJ, Maeng JH, Hwang SY et al (2018) Design, fabrication, and testing of a microfluidic device for thermotaxis and chemotaxis assays of sperm. SLAS Technol 23(6):507–515. https://doi.org/10.1177/2472630318783948
22. Soto-Heras S, Sakkas D, Miller DJ (2023) Sperm selection by the oviduct: perspectives for male fertility and assisted reproductive technologies. Biol Reprod 108(4):538–552. https://doi.org/10.1093/biolre/ioac224
23. Sequeira RC, Criswell T, Atala A et al (2020) Microfluidic systems for assisted reproductive technologies: advantages and potential applications. Tissue Eng Regen Med 17(6):787–800. https://doi.org/10.1007/s13770-020-00311-2
24. Sharma S, Kabir MA, Asghar W (2022) Selection of healthy sperm based on positive rheotaxis using a microfluidic device. Analyst 147(8):1589–1597. https://doi.org/10.1039/d1an02311j
25. Teves ME, Roldan ERS (2022) Sperm bauplan and function and underlying processes of sperm formation and selection. Physiol Rev 102(1):7–60. https://doi.org/10.1152/physrev.00009.2020
26. Vasilescu SA, Ding L, Parast FY et al (2023) Sperm quality metrics were improved by a biomimetic microfluidic selection platform compared to swim-up methods. Microsyst Nanoeng 9:37. https://doi.org/10.1038/s41378-023-00501-7
27. Ahmadkhani N, Hosseini M, Saadatmand M et al (2022) The influence of the female reproductive tract and sperm features on the design of microfluidic sperm-sorting devices. J Assist Reprod Genet 39(1):19–36. https://doi.org/10.1007/s10815-021-02377-w
28. Suarez SS, Wu M (2017) Microfluidic devices for the study of sperm migration. Mol Hum Reprod 23(4):227–234. https://doi.org/10.1093/molehr/gaw039
29. Penny JA, Lymbery RA, Evans JP et al (2022) The use of microfluidic devices in studies of differential sperm chemotaxis. Trends Biotechnol 40(10):1144–1147. https://doi.org/10.1016/j.tibtech.2022.06.014
30. Bahat A, Eisenbach M (2006) Sperm thermotaxis. Mol Cell Endocrinol 252(1–2):115–119. https://doi.org/10.1016/j.mce.2006.03.027
31. Romero-Aguirregomezcorta J, Laguna-Barraza R, Fernández-González R et al (2021) Sperm selection by rheotaxis improves sperm quality and early embryo development. Reproduction 161(3):343–352. https://doi.org/10.1530/rep-20-0364
32. Guler C, Melil S, Ozekici U et al (2021) Sperm selection and embryo development: a comparison of the density gradient centrifugation and microfluidic chip sperm preparation methods in patients with astheno-teratozoospermia. Life 11(9):933. https://doi.org/10.3390/life11090933
33. Bahat A, Caplan SR, Eisenbach M (2012) Thermotaxis of human sperm cells in extraordinarily shallow temperature gradients over a wide range. PLoS ONE 7(7):e41915. https://doi.org/10.1371/journal.pone.0041915
34. Bahat A, Tur-Kaspa I, Gakamsky A et al (2003) Thermotaxis of mammalian sperm cells: a potential navigation mechanism in the female genital tract. Nat Med 9(2):149–150. https://doi.org/10.1038/nm0203-149
35. Boryshpolets S, Pérez-Cerezales S, Eisenbach M (2015) Behavioral mechanism of human sperm in thermotaxis: a role for hyperactivation. Hum Reprod 30(4):884–892. https://doi.org/10.1093/humrep/dev002
36. Bahat A, Eisenbach M (2010) Human sperm thermotaxis is mediated by phospholipase c and inositol trisphosphate receptor Ca^{2+} channel. Biol Reprod 82(3):606–616. https://doi.org/10.1095/biolreprod.109.080127
37. Eisenbach M, Giojalas LC (2006) Sperm guidance in mammals—an unpaved road to the egg. Nat Rev Mol Cell Biol 7(4):276–285. https://doi.org/10.1038/nrm1893
38. Ahmad R, Dalziel JE (2020) G protein-coupled receptors in taste physiology and pharmacology. Front Pharmacol 30(11):587664. https://doi.org/10.3389/fphar.2020.587664
39. Cygankiewicz AI, Maslowska A, Krajewska WM et al (2014) Molecular basis of taste sense: involvement of GPCR receptors. Crit Rev Food Sci Nutr 54(6):771–780. https://doi.org/10.1080/10408398.2011.606929
40. Toni LD, Garolla A, Menegazzo M et al (2016) Heat sensing receptor TRPV1 is a mediator of thermotaxis in human spermatozoa. PLoS ONE 11(12):e0167622. https://doi.org/10.1371/journal.pone.0167622
41. Hamano KI, Kawanishi T, Mizuno A et al (2016) Involvement of transient receptor potential vanilloid (TRPV) 4 in mouse sperm thermotaxis. J Reprod Dev 62(4):415–422. https://doi.org/10.1262/jrd.2015-106
42. Fujinoki M (2012) Progesterone-enhanced sperm hyperactivation through IP_3–PKC and PKA signals. Reprod Med Biol 12(1):27–33. https://doi.org/10.1007/s12522-012-0137-6
43. Fotiadis D, Liang Y, Filipek S et al (2003) Rhodopsin dimers in native disc membranes. Nature 421(6919):127–128. https://doi.org/10.1038/421127a
44. Dhaka A, Viswanath V, Patapoutian A (2006) TRP ion channels and temperature sensation. Annu Rev Neurosci 29:135–161. https://doi.org/10.1146/annurev.neuro.29.051605.112958
45. Nakao S, Takeo T, Watanabe H et al (2020) Successful selection of mouse sperm with high viability and fertility using microfluidics chip cell sorter. Sci Rep 10(1):8862. https://doi.org/10.1038/s41598-020-65931-z
46. Ruiz-Díaz S, Oseguera-López I, Cuesta-Díaz DDL et al (2020) The presence of D-penicillamine during the in vitro capacitation of stallion spermatozoa prolongs hyperactive-like motility and allows for sperm selection by thermotaxis. Animals 10(9):1467. https://doi.org/10.3390/ani10091467
47. Xiao W, Yu M, Yuan Y et al (2022) Thermotaxis of mammalian sperm. Mol Hum Reprod 28(8):gaac027. https://doi.org/10.1093/molehr/gaac027

48. Yan Y, Zhang B, Fu Q et al (2021) A fully integrated biomimetic microfluidic device for evaluation of sperm response to thermotaxis and chemotaxis. Lab Chip 21(2):310–318. https://doi.org/10.1039/d0lc00845a